Opto-Electronics Review

journal homepage: https://journals.pan.pl/opelre

Experimental and theoretical studies of Znq_2 thin film fabricated by spin-coating and its characterisation as an active layer in OLED

Malgorzata Sypniewska[1,2*], Iulia E. Brumboiu[2], Anna Kaczmarek-Kedziera[3], Monika Pokladko-Kowar[4], Ewa Gondek[4], Pawel Popielarski[5], Robert Szczesny[3], Beata Derkowska-Zielinska[2**]

[1] Division of Surface Science, Faculty of Chemical Technology and Engineering, Bydgoszcz University of Science and Technology, Al. Prof. S. Kaliskiego 7, 85-796 Bydgoszcz, Poland

[2] Institute of Physics, Faculty of Physics, Astronomy and Informatics, Nicolaus Copernicus University in Toruń, ul. Grudziądzka 5, Toruń 87-100, Poland

[3] Faculty of Chemistry, Nicolaus Copernicus University in Toruń, ul. Gagarina 7, Toruń 87-100, Poland

[4] Department of Physics, Cracow University of Technology, ul. Podchorążych 1, 30-084 Kraków, Poland

[5] Department of Physics, Kazimierz Wielki University in Bydgoszcz, ul. Powstańców Wielkopolskich 2, 85-090 Bydgoszcz, Poland

Article info

Article history:
Received 13 Dec. 2024
Received in revised form 18 Apr. 2025
Accepted 15 May 2025
Available on-line 16 Jul. 2025

Keywords:
thin films;
bis(8-hydroxyquinoline) zinc;
photoluminescence;
electroluminescence;
organic light-emitting diodes.

Abstract

Bis(8-hydroxyquinoline) zinc dispersed in a poly(N-vinylcarbazole) matrix (Znq_2:PVK) was characterised for its possible use as an active layer in organic light-emitting diodes. The composition and morphology of Znq_2:PVK thin films deposited on quartz substrates was analysed by Fourier transform infrared spectroscopy (FTIR), scanning electron microscopy (SEM), and confocal microscopy. Optical properties of the films were characterised by absorption spectroscopy and photoluminescence and explained on the basis of calculated molecular properties of gas phase Znq_2, N-vinylcarbazole pentamer, and molecular models for the Znq_2:PVK interface. FTIR measurements of the Znq_2:PVK film revealed the presence of water, likely due to the formation of Znq_2-dihydrate during the fabrication process. Water could be removed by annealing films at 130 °C for 1 h and the annealed films showed better photoluminescence in the Znq_2 emission region. Finally, two diodes with an ITO/PEDOT:PSS/Znq_2:PVK/Al structure were fabricated, where in the second one, the ITO/PEDOT:PSS/Znq_2:PVK layers were annealed at 130 °C. The first diode was characterised by a maximum brightness of about 83 cd/m^2 and a current efficiency of 0.12 cd/A, while the diode whose structure was annealed had a maximum brightness of about 219 cd/m^2 and a current efficiency of 0.26 cd/A.

1. Introduction

Bis(8-hydroxyquinoline) zinc (Znq_2) is one of the metal chelates Mq_m (where m is the oxidation state of the metal – M) [1], which is a good candidate for improving the luminescent properties of organic light-emitting diodes (OLEDs) [2–7]. The Znq_2 has better electron transport properties compared to Alq_3 (tris(8-hydroxyquinoline) aluminium), resulting in lower operating voltages of the corresponding OLED devices [8]. Additionally, Znq_2 has higher thermal stability compared to other transport layers [9], and Znq_2-based OLEDs are relatively more stable under the influence of high operating voltages [10, 11]. That is, changing the operating voltage does not significantly affect their electroluminescence (EL) [8].

Znq_2 can occur in two forms, each with distinct properties. Under anhydrous conditions, it forms tetramers consisting of four Znq_2 ($(Znq_2)_4$) molecules bridged by

Corresponding author at: *malgorzata.sypniewska@pbs.edu.pl
**beata@fizyka.umk.pl

https://doi.org/10.24425/opelre.2025.154747
1896-3757/ Association of Polish Electrical Engineers (SEP) and Polish Academic of Sciences (PAS). Published by PAS

oxygen atoms [12, 13]. The planar structure of $(Znq_2)_4$ leads to a higher electron mobility, resulting in lower turn-on voltages in OLEDs mentioned above. Additionally, in presence of water, Znq_2 can occur as a dihydrate containing two water molecules ($Znq_2 \cdot 2H_2O$) aligned axially concerning the Zn atom with two hydroxyquinoline ligands in the plane [14]. The formation of the Znq_2 dihydrate generally suppresses light emission and deteriorates device performance [15]. In contrast to the pure Znq_2, which provides excellent electronic and optical properties, as well as good relative stability, the Znq_2 dihydrate is not suitable for OLED applications.

Several groups have prepared OLEDs based on Znq_2 in various device architectures, yielding significantly different OLED characteristics. Emission peaks at 556 nm were obtained for Znq_2-based OLED structures such as ITO/PEDOT:PSS/PVK/Znq_2/PBD/Al and ITO/PEDOT:PSS/PVK:Znq_2:PBD/Al [16]. These were shown to have lower turn-on voltages and higher current densities compared to Alq_3 OLEDs in the same configuration [16]. Others obtained emission peaks at 530 nm (ITO/Znq_2:PVK/Al) [12], or 540 nm (ITO/PEDOT:PSS/NPB/Znq_2/BCP/LiF/Al) [17]. The maximum measured brightness of these different OLEDs also varied drastically. A maximum brightness of 791 cd/m^2 was obtained by Rawat *et al*. for ITO/PEDOT:PSS/NPB/Znq_2/BCP/LiF/Al [17], while a brightness of 3000 cd/m^2 was noticed by Lim *et al*. for an OLED with an ITO/TPD:PMDA-ODA PI/Znq_2/Al structure [18]. The highest brightness ever obtained for Znq_2-based devices was 16 200 cd/m², achieved by Sano *et al*. for ITO/TPD/Znq_2/Al [19]. These large variations in brightness may likely be related to the differences in properties between Znq_2-dihydrate and pure Znq_2.

This work aims to present the optical and structural properties of a bis(8-hydroxyquinoline) zinc poly(N-vinylcarbazole) (Znq_2:PVK) thin film, deposited on quartz substrates by spin-coating, using Fourier transform infrared spectroscopy (FTIR), scanning electron microscopy (SEM), confocal microscopy (CM), ultraviolet-visible (UV-Vis), and photoluminescence (PL). Using FTIR spectroscopy, the authors show that the thin films contain water, probably due to the formation of Znq_2-dihydrate. Annealing these films at 130 °C for 1 h should result in the removal of water and the formation of Znq_2 tetramers. This hypothesis is confirmed by PL measurements and UV-Vis absorption spectroscopy combined with time-dependent density functional theory calculations for the gas-phase Znq_2, Znq_2-dihydrate, Znq_2 tetramers, PVK, and Znq_2:PVK model systems. The authors has also prepared a simple OLED structure (i.e., ITO/PEDOT:PSS/Znq_2:PVK/Al) which, to the best of their knowledge, is the first such structure with Znq_2:PVK as an active layer.

2. Materials and methods

2.1. Materials

Znq_2 and poly N-vinylcarbazole (PVK, M_w ~1 000 000 g/mol) powders were purchased from Sigma-Aldrich. The molecular structures of Znq_2 and PVK are presented in Fig. 1(a).

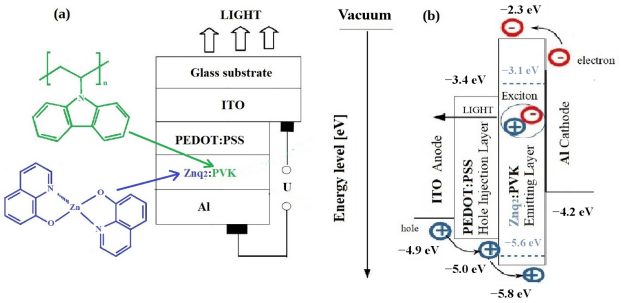

Fig. 1. (a) OLED structure with Znq_2 and PVK molecular structures (ITO$_{(L = 118{,}35\ nm)}$/PEDOT:PSS$_{(L = 60\ nm)}$/Znq_2:PVK$_{(L = 109{,}90\ nm)}$/Al$_{(L = 103\ nm)}$) and (b) its energy levels.

2.2. Thin films preparation

To obtain a Znq_2:PVK thin layer on a quartz substrate by spin-coating (Spin coater Laurell, 1600 rpm), PVK was first dissolved in dichloroethane (for HPLC ≥ 99.8%, Sigma Aldrich), and after 24 h, 20 mg of Znq_2 powder was added. This mixture was then placed in an ultrasonic bath for approximately 30 min before being deposited on a clean substrate [20]. Additionally, a Znq_2:PVK thin layer was annealed for one hour at 130 °C in a muffle furnace.

2.3. Experimental methods

FTIR spectra of Znq_2:PVK thin films before and after annealing at 130 °C were measured using an FT-IR Vertex 70 V with a Hyperion 1000/2000 microscope from Bruker Optik in the range of 200–1800 cm^{-1}. SEM measurements were performed with a Quanta 3D FEG (EHT = 30 kV) instrument. Confocal microscopy measurements were performed using a Lext Olympus OLS 4000 device with a 405 nm laser. In this article, 20× magnification was used, and the imaged area size was 645 × 645 μm^2. UV-Vis measurements of Znq_2:PVK thin films deposited on quartz substrates before and after annealing at 130 °C were measured at room temperature using a Specord 200 spectrometer in the range of 270–600 nm. The PL signal of Znq_2:PVK thin films before and after heating was registered using an FS5 spectrofluorometer.

2.4. OLED

The procedure for fabricating the following ITO/PEDOT:PSS/Znq_2:PVK/Al OLED structure [see Fig. 1(a)] is described elsewhere [20]. The energy band diagram of the prepared OLED is shown in Fig. 1(b). In this structure, a glass substrate is used as a support for the OLED. Transparent indium tin oxide (ITO) serves as an anode, providing light transmission. When a voltage is applied to the OLED electrodes, holes are transported from the ITO and injected into the Znq_2:PVK emitting layer *via* PEDOT:PSS, a layer that facilitates the injection of holes from ITO into Znq_2:PVK. At the same time, electrons are transported from the cathode (Al) and injected into the emitting layer. As a result, electron-hole pairs recombine in Znq_2:PVK and light is emitted as long as current flows.

2.5. *Theoretical calculations*

The molecular structures of Znq_2, Znq_2-dihydrate ($Znq_2 \cdot 2H_2O$), and the Znq_2 tetramer ($(Znq_2)_4$) were optimized in Gaussian16 [21] at the density functional theory (DFT) level using the ωB97X-D functional [22] in combination with the def2-SVP basis set [23].

The stable conformations of the Znq_2:PVK models were determined with the introductory metadynamics run with the XTB program by Grimme [24]. The geometry of the resulting structures was reoptimized with the ωB97X-D/def2-SVP approach and the character of the stationary points was confirmed with a harmonic vibrational analysis (see Fig. 2). The structures exhibiting relative energies below 3 kcal/mol were investigated, since they may be important components of the reaction mixture under standard conditions. However, the final calculations were carried out only for the most stable configurations, since the structures, interaction energy, and photophysical properties were similar for all these molecular systems. The vertical absorption was investigated within time-dependent (TD)-DFT with the ωB97X-D functional [22]. This choice of a functional is dictated by its confirmed general good performance both for structure and excitation energy in the case of organic dyes. The long-range corrected ωB97X-D functional, combined with the empirical Grimme dispersion correction, ensures a good balance between the computational cost and quality of calculations for the polymer models investigated here. The energies of frontier orbitals were also predicted using the HSE06 functional to maintain consistency with the authors' previous work on the Alq_3:PVK systems [20]. To deeply analyse the character of the excitations, Le Baher's charge transfer indexes were calculated [25]. The supermolecular interaction energy with the counterpoise correction was estimated within the ωB97X-D/def2-SVP approach. All DFT calculations were carried out with the Gaussian16 program [21] and non-covalent interactions were depicted with NCIPlot [26–28].

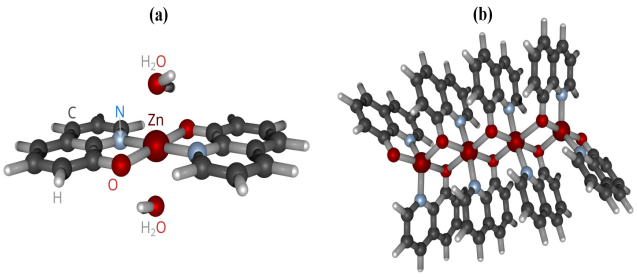

Fig. 2. Optimized geometry of (a) $Znq_2 \cdot 2H_2O$ and (b) $(Znq_2)_4$.

3. Results and discussion

The absorption spectra of Znq_2:PVK thin films deposited on a quartz substrate before and after annealing at 130 °C are shown in Fig. 3(a). It can be observed that for Znq_2:PVK thin layers, there are three absorption bands. The first one, located at 294 nm, is assigned to the optical transitions of carbazole units of PVK [29]. The band at 334 nm (before annealing) is assigned to a π–π* excitation of the 8-hydroxyquinoline unit, while the band at 344 nm

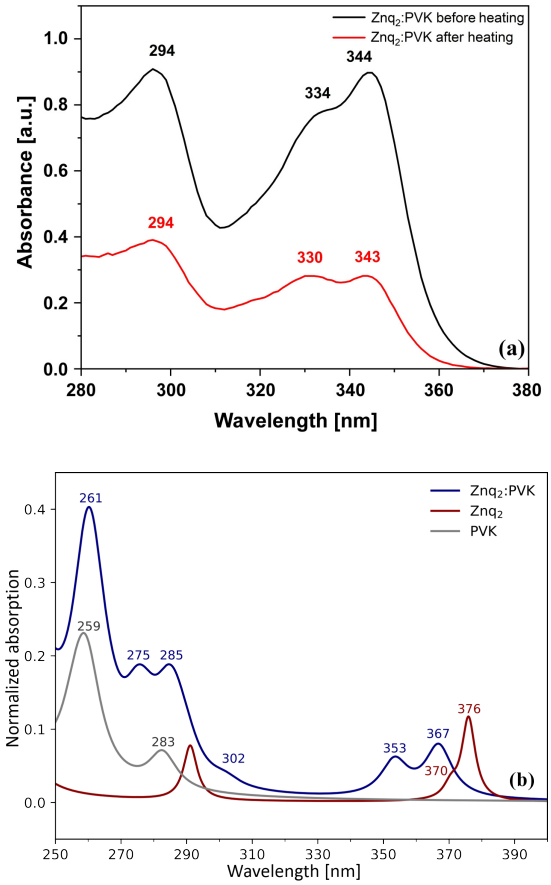

Fig. 3. (a) Absorption spectra of Znq_2:PVK thin films before and after annealing at 130 °C. (b) Vertical absorption spectrum for Znq_2 (red line), PVK model (grey line), and Znq_2:PVK (blue line) estimated with the TD-ωB97X-D/def2-SVP approach. See also Fig. S2 in the Supporting Information (SI).

(before annealing) is also an excitation of π–π* character, but involving two other π orbitals of the 8-hydroxyquinoline unit [30, 31] [the natural transition orbitals (NTOs) and related discussion is below and in SI]. A slight shift of these bands to 330 nm, respectively 343 nm, is observed after annealing.

The vertical absorption spectrum for a single Znq_2 molecule in vacuum and for a Znq_2:PVK model, calculated within the TD-ωB97X-D/def2-SVP approach, is presented in Fig. S2. The lowest energy bands at 376 nm and 370 nm in bare Znq_2 become shifted hypsochromically by about 10–20 nm upon interaction with PVK. These calculated peaks for the Znq_2:PVK model system correspond to the absorption bands measured experimentally at 343 nm and 330 nm (after annealing). It is worth noting that the authors' theoretical model is limited to one Znq_2 molecule relaxed in the vicinity of a PVK oligomer containing five repeated monomer units. The shifts (of about 20–25 nm, or 0.15–0.4 eV) observed between the calculated and measured bands are of the same order of magnitude as the accuracy of the TD-DFT approach using ωB97X-D functional [32] and are reasonable considering the limited molecular model used to represent the Znq_2:PVK interface. The corresponding natural transition orbitals of Znq_2, depicted in panel Fig. S3(a), reveal that the character of these transitions is π→π* with the corresponding electron density concentrated at the 8-hydroxyquinoline moiety.

The wavelength region between 250 nm and 300 nm is somewhat more complicated, as transitions can be observed involving charge transfer between Znq_2 and a polymer chain (see NTOs in Fig. S3 in the SI). However, the strong band calculated at 261 nm can be attributed mainly to the polymer, as indicated by the NTOs depicted in Fig. S3. Considering the accuracy of the authors' theoretical model, the bands calculated in the 250–300 nm region can be assigned to the measured band centred at 294 nm.

The structure of the Znq_2:PVK model obtained within DFT approach indicates strong π-π stacking between the 8-hydroxyquinoline moiety of Znq_2 and carbazole rings in the polymer chain (see Fig. 4). The Znq_2 molecule fits well between aromatic side substituents of the polymer to maximize the mutual attraction. For the model polymer chain and Znq_2, the counterpoise-corrected supermolecular interaction energy is equal to −35.78 kcal/mol in the case of the most stable configuration. This is more than 5 kcal/mol stronger than an interaction observed for the similar Alq_3:PVK interface [20], where a similar arrangement leads to an interaction energy equal to −23.29 kcal/mol for the mer-Alq_3:PVK complex. This enhancement of the attraction arises from better compatibility of the Znq_2 shape to the arrangement of carbazole aromatic units in the polymer chain than that observed for the three perpendicular hydroxyquinoline modules in Alq_3.

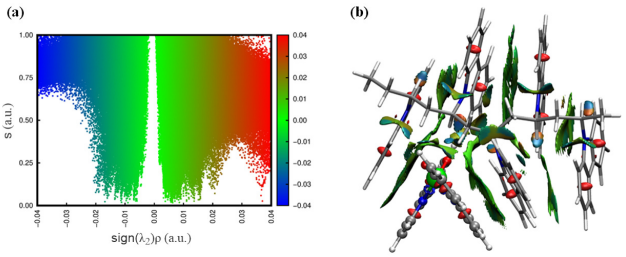

Fig. 4. (a) NCIPlot weak interaction analysis with colour-coding blue for strong attractive interactions, green for weak van der Waals interactions, and red for repulsion; (b) lowest energy configuration of Znq_2:PVK complex optimized within the ωB97X-D/def2-SVP approach together with the surfaces indicating the intramolecular and intermolecular interactions, according to NCIPlot (polymer chain presented as licorice and Znq_2 molecule – in CPK representation; green isosurfaces indicate weak van der Waals interactions).

Theoretical values of HOMO and LUMO energies for model PVK, Znq_2, and the Znq_2:PVK system are presented in Fig. 5 together with the shape of the corresponding orbitals. The comparison with the Alq_3:PVK [20] material shows an even better match between the polymer HOMO energy and Znq_2 LUMO energy, which is slightly lowered with respect to the isolated Alq_3 LUMO level.

The FTIR spectrum was recorded for the purchased Znq_2 powder to determine its crystalline form. The spectrum shown in Fig. 6(a) clearly indicates that the compound exists in the anhydrous form. The FTIR spectrum for the dihydrate phase would have an additional broad band at 3200 cm^{-1}, which is not visible in this spectrum. FTIR spectra were measured for Znq_2 films obtained by spin-coating after the solvent (dichloroethane) was allowed to evaporate. In the case of the layer deposited on the substrate without any subsequent thermal treatment [see Fig. 6(b)],

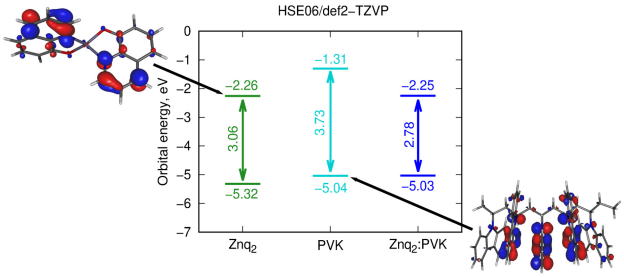

Fig. 5. Orbital energy levels for HOMO and LUMO orbitals of Znq_2, PVK, and Znq_2:PVK estimated with HSE06/def2-TZVP.

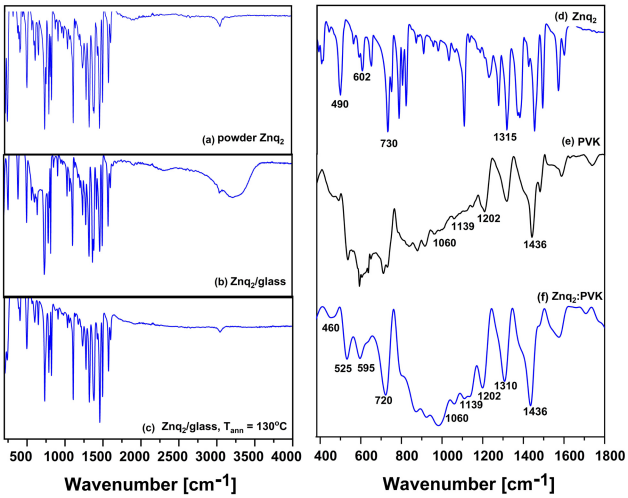

Fig. 6. FTIR spectra for powder of (a) Znq_2 and (b) thin films of Znq_2 on glass before and (c) after annealing at 130 °C, and (d) layers of Znq_2, (e) PVK, and (f) Znq_2:PVK.

Znq_2 occurred in a dihydrate form ($Znq_2 \cdot 2H_2O$), as evidenced by the presence of a broad O–H band appearing in the range of 3000–3300 cm^{-1}. The sample was then annealed at 130 °C. This temperature was selected to achieve a phase transition from $Znq_2 \cdot 2H_2O$ dihydrate to anhydrous $(Znq_2)_4$ [15]. FTIR measurements were repeated for the layer after annealing at 130 °C [see Fig. 6(c)], and anhydrous Znq_2 was obtained, similarly to the starting powder used to prepare the deposition mixture [Fig. 6(a)]. Figures 6(e) and 6(f) show the FTIR spectra of PVK and Znq_2:PVK thin films in the range of 400–1800 cm^{-1}. The peaks at 400–600 cm^{-1} are assigned to Zn–O and Zn–N stretching vibrations, while the peaks at about 595 and 720 cm^{-1} are assigned to in-plane ring deformations [33]. Characteristic bands appear for the PVK polymer at: 1060 cm^{-1}, 1139 cm^{-1}, 1202 cm^{-1}, and 1436 cm^{-1} [34]. The vibrations at 1310 cm^{-1} are assigned instead to the quinoline group of Znq_2 [35].

Comparing PVK to Znq_2:PVK, it can be seen that the FTIR bands corresponding to the polymer are located at the same wavenumbers in both samples. However, comparing Znq_2 to Znq_2:PVK, shifts are observed for some of the bands. In the case of the bands in the range of 400–600 cm^{-1} associated with Zn–O and Zn–N stretching vibrations, they become weaker after the formation of the Znq_2:PVK structure. The Znq_2 band at 730 cm^{-1}, corresponding to in-plane ring deformations, is shifted to 720 cm^{-1} in Znq_2:PVK. Similarly, the Znq_2 band at 1315 cm^{-1}, assigned to vibrations

of the quinoline group, is shifted to 1310 cm^{-1} in the Znq_2:PVK sample.

Bakhshipour *et al.* [36] studied Znq_2 annealed at temperatures of 50, 100, 150, and 200 °C. They observed a transition from $(Znq_2)\cdot 2H_2O$ to $(Znq_2)_4$ at higher annealing temperatures based on the disappearance of the O-H band at 3400 cm^{-1}. Painuly *et al.* [15] observed a change from (Znq_2) $2H_2O$ to $(Znq_2)_4$ after annealing in argon for 3 h at 200 °C, while Hu *et al.* [37] showed that the transition from dihydrate to anhydrous Znq_2 began at 135 °C in vacuum.

Figure 7 shows the PL spectra of Znq_2:PVK thin films on a quartz substrate before and after annealing at 130 °C for three different excitation wavelengths: 296 nm, 344 nm, and 440 nm. Two distinct peaks are visible in the spectra. The first peak for the unannealed sample, appearing at 413 nm, corresponds to PVK and is related to intrachain excimers comprising different configurations of two adjacent carbazole groups [38]. These excimers arise from the interaction between excited states of neighbouring carbazole units, resulting in a characteristic emission wavelength. The formation and stability of these excimers are influenced by the polymer matrix and the spatial arrangement of the carbazole units. The second peak, observed in the sample before annealing, is in the range of 505–510 nm and corresponds to Znq_2. This peak is attributed to the electron intraligand charge transfer (ILCT) transition within the Znq_2. The electron transitions are π-π* and are related to the $S_1 \rightarrow S_0$ transitions of the Znq_2 [3]. The ILCT transition involves the transfer of an electron from a ligand-centred orbital to another ligand-centred orbital, which is influenced by the molecular structure and the surrounding matrix.

Upon annealing, the spectra reveal significant changes. The peaks shift to 405 nm for PVK and to 538 nm for excitations at 296 and 344 nm, and to 560 nm for excitation at 440 nm for Znq_2. These shifts can be explained by the structural changes induced by heating. Before annealing, the films contain the $Znq_2\cdot 2H_2O$ form in which water molecules are loosely bound to the zinc atom. Heating to 130 °C removes these water molecules, leading to the formation of an anhydrous Znq_2, which tends to form a tetrameric structure $(Znq_2)_4$. This structural transformation alters the electronic environment of the Znq_2 molecules, leading to distinct emission properties.

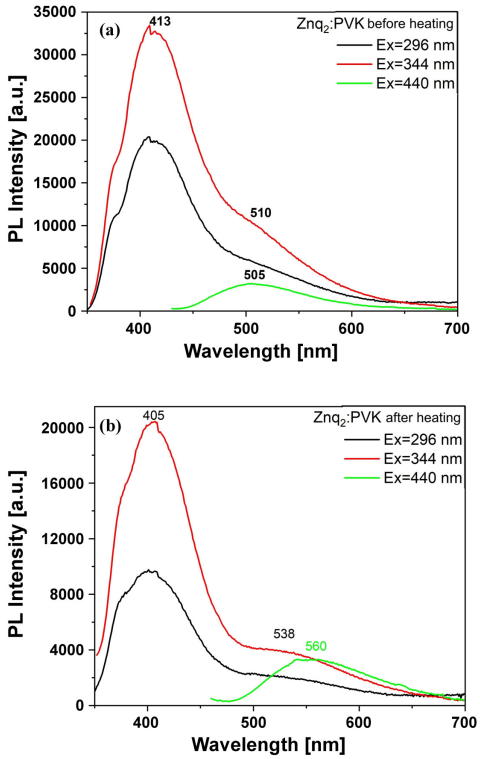

Fig. 7. PL spectra of thin film of Znq_2 dispersed in PVK matrices (a) before and (b) after annealing at 130 °C.

In the work of Hopkins *et al.* [12], the PL results for Znq_2 and Znq_2 dispersed in a PVK polymer matrix were compared. They found that the maximum PL peak for Znq_2 was at 542 nm, while in the PVK matrix, the PL spectrum maximum shifted to 528 nm. This shift is consistent with the electron-withdrawing nature of the sulphonamide substituent. The presence of the PVK matrix affects the electronic interactions within the Znq_2, leading to a shift in the emission wavelength.

Additionally, it is noteworthy that the highest spectral intensity was achieved at an excitation wavelength of 296 nm which decreases as the excitation wavelength increases. This variation can be attributed to the excitation efficiency and the overlap between the excitation wavelength and the absorption spectrum of the material. As the excitation wavelength increases, the overlap decreases, resulting in lower PL intensity. Moreover, an increase in the excitation value results in a shift of the PL peak. This phenomenon of shifting PL maxima with changes in excitation wavelength is characteristic of metalloquinolines. This behaviour is based on the coupling of vibrations of individual ligands with fluorescence transitions [39, 40]. The vibrational states of ligands can interact with electronic transitions, leading to a shift in the emission wavelength. Metalloquinoline molecules possess a specific geometric configuration and uniform energy levels which can restrict their vibrational freedom. During excitation, only molecules with energy levels corresponding to the excitation wavelength are excited, resulting in the observed shift of the PL peak [41].

SEM and confocal microscopy image analyses for the Znq_2:PVK sample are shown in Figs. 8(a) and 8(b). SEM measurement reveals that the obtained thin layer is relatively smooth, with some agglomerates present. The aggregation of Znq_2 may be attributed to intermolecular interactions such as π–π stacking, C–H···O hydrogen bonding, and C–H···π interactions between the molecules [35]. The sizes of such agglomerates range from 20 to 50 µm. Figure 8(b) shows that the polymer layer is inhomogeneous near the agglomerates. In addition to the agglomerates, smaller Znq_2 grains are visible.

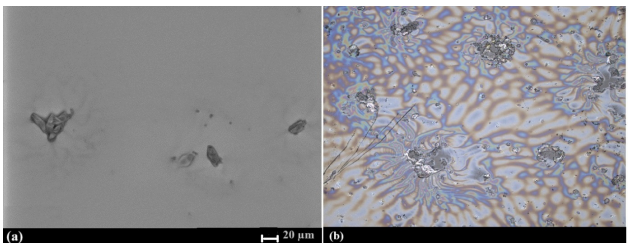

Fig. 8. SEM image of the Znq_2:PVK surface (a) at magnification 500x; (b) confocal microscope photo at magnification 20x; image size 645 × 645 μm^2.

The refractive index (n) and extinction coefficient (k) obtained from spectroscopic ellipsometry measurements for the OLED structure studied in this work are shown in Fig. 9. The results are similar to those presented by the authors in [42] for the Znq_2 derivative with a styryl group. The angles Δ and Ψ obtained experimentally and measured for different illumination angles ranging from 60° to 70°, are presented in Fig. S4.

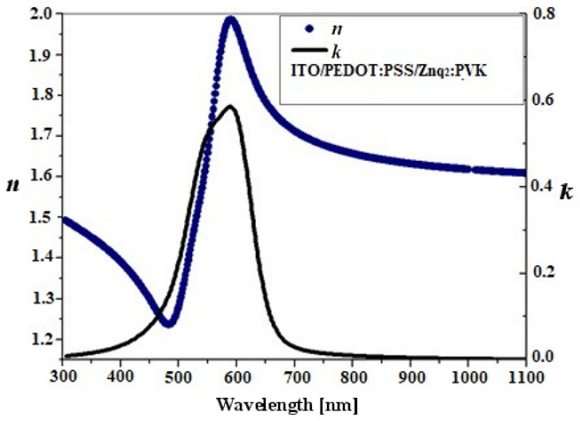

Fig. 9. Dependence of n and k for the unannealed Znq_2:PVK layer on a PEDOT:PSS/ITO/glass substrate.

Figures 10(a) and 10(b) show the current density-voltage and the EL-voltage curves, respectively. Figure 10(a) shows the current-voltage characteristics of the studied OLED before and after annealing the Znq_2:PVK layer. The threshold voltage U_T was 8.94 V and 9.36 V for the diode before and after annealing the Znq_2:PVK film at 130 °C, respectively. The EL-voltage characteristics presented in Fig. 10(b) show typical features of EL devices. The tested OLED before annealing exhibits a maximum brightness value of approximately 83 cd/m² with a current efficiency of 0.12 cd/A. In the case of the diode in which the Znq_2:PVK film was annealed, the maximum brightness value of about 219 cd/m^2 was obtained with a current efficiency of 0.26 cd/A. The presence of water in the diode before annealing may be responsible for the low parameters of the OLED. It can be seen that after annealing, the maximum brightness value increased more than twice, which may confirm this thesis.

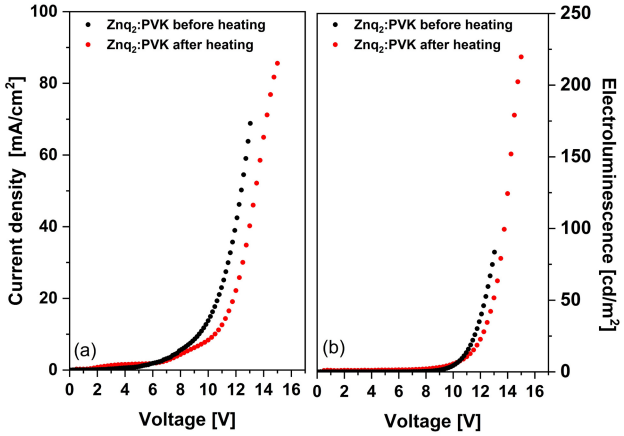

Fig. 10. (a) Current density-voltage curves and (b) EL-voltage characteristics for structure ITO/PEDOT:PSS/Znq_2:PVK/Al, where Znq_2:PVK was not annealed and after being annealed.

The diode obtained is weaker than the Znq_2 diodes described by other authors. This may be due to a different method of depositing the Znq_2 layer, as well as the presence of additional layers that have not been included which may support carrier transfer in the diode, leading to better parameters. Rawat *et al*. described an OLED with an ITO/PEDOT structure: PSS (40 nm)/NPB (20 nm)/Znq_2 (50 nm)/BCP (7 nm)/LiF (0.8 nm)/Al (200 nm), where the active layer was deposited in high vacuum [17]. The diode they obtained was characterised by maximum EL at a wavelength of 540 nm with a maximum current efficiency of 0.64 cd/A and a maximum brightness of 791 cd/m^2. Sano *et al.* [19] prepared an OLED with an ITO/TPD (50 nm)/Znq_2/Al architecture in which the emission layer was deposited in a vacuum gas phase as above. The maximal brightness value of 16 200 cd/m^2 obtained by the authors is the highest value ever measured for Znq_2. Lim *et al*. [18] modified the TPD/Znq_2 structure and proposed the an ITO/TPD:PMDA-ODA PI/Znq_2/Al structure where PMDA-ODA P1 was used as a matrix polymer binding the HTM. The emission layer was thermally evaporated and the maximum brightness value obtained was higher than that of the authors and amounted to 3000 cd/m². Burlov *et al.* [43] presented an OLED containing a Znq_2 derivative with an ITO/PEDOT: PSS/mCp/zinc complex/ TPDI/LiF/Al structure which was characterised by a maximum brightness of 2103 cd/m^2 and a maximum emission band in the range of 478–490 nm. Other Znq_2 derivatives were presented by Moraes *et al.* [44] (ITO/PEDOT:PSS/ PVK/zinc complex/ TmPyPB/Ca/Al). These diodes had a maximum brightness between 536 and 668 cd/m² which is higher than the authors' reported value.

4. Conclusions

In this paper, Znq_2:PVK thin films were prepared for their potential use in OLED applications and their optical and morphological properties were investigated. From the FTIR spectra, it was observed that the Znq_2 molecule tends to form a dihydrate complex. The dissolution of this complex and its rapid recrystallization during layer formation cause changes in the coordination environment of the central atom. By annealing the films at 130 °C for 1 h, it was possible to remove water and restore Znq_2 to its anhydrous form.

In the case of PL measurements, a significant shift of a Znq_2 emission maximum from 505 nm to 550 nm was observed for the annealed sample. The changes and variations in the obtained PL spectra can be explained by: i) formation of an intrachain excimer due to the interaction between excited states of neighbouring carbazole units in PVK, ii) ILCT transition involving electron intraligand charge transfer in Znq_2 under influence of the molecular structure and the surrounding matrix, iii) structural transformation of $Znq_2 \cdot 2H_2O$ into anhydrous Znq_2 tetramer caused by annealing, iv) changes in PL intensity with excitation wavelength due to the overlap between excitation and absorption spectra, and v) vibrational coupling between the vibrational states of ligands and electronic transitions causing shifts of the PL peaks.

The structure of the Znq_2:PVK system obtained by the DFT method indicates a strong π-π stacking between the 8-hydroxyquinoline moiety of Znq_2 and the carbazole rings in the polymer chain.

The authors have found that the ITO/PEDOT:PSS/Znq_2:PVK/Al OLED structure, where the Znq_2:PVK layer was not annealed, showed a maximum brightness value of about 83 cd/m^2 with CE 0.12 cd/A. The presence of water may be the reason for such low OLED parameters. This thesis was confirmed for the ITO/PEDOT:PSS/Znq_2:PVK/Al structure, where the Znq_2:PVK layer was annealed at 130 °C. For the annealed OLED, the maximum brightness value was about 219 cd/m^2 with CE 0.26 cd/A. The obtained diode has lower parameters compared to other Znq_2 diodes described by other authors likely due to its structure and the method of manufacturing the active layers. Future work is planned to improve these parameters by adding additional layers supporting charge transport.

Authors' statement

Research concept and design: M.S., R.S., and B.D.-Z.; collection and/or assembly of data: M.S., I.E.B., A.K.-K., M.P.-K., E.G., P.P., R.S., and B.D.-Z.; data analysis and interpretation: M.S., I.E.B., A.K.-K., E.G., P.P., R.S., and B.D.-Z.; writing the article: M.S., A.K.-K., and I.E.B.; critical revision of the article: R.S. and B.D.-Z.; final approval of article: M.S., I.E.B., A.K.-K., E.G., P.P., R.S., and B.D.-Z.

References

[1] Tsuboi, T. & Torii, Y. Selective synthesis of facial and meridional isomers of Alq_3. *Mol. Cryst. Liq. Cryst.* **529**, 42–52 (2010). https://doi.org/10.1080/15421406.2010.495672

[2] Painuly, D., Masram, D. T., Rabanal, M. E. & Nagpure, I. M. The effect of ethanol on structural, morphological and optical properties of Li(I) 8–hydroxyquinoline phosphor. *J. Lumin.* **192**, 1180–1190 (2017). https://doi.org/10.1016/j.jlumin.2017.08.054

[3] Painuly, D., Singhal, R., Kandwal, P. & Nagpure, I .M. Structural, optical and decay properties of zinc(II) 8-hydroxyquinoline and its thin film. *J. Electron. Mater.* **49**, 6096–6106 (2020). https://doi.org/10.1007/s11664-020-08255-y

[4] Pérez-Bolivar, C. P., Takizawa, S., Nishimura, G., Montes, V. A. & Anzenbacher, P. Jr. High-efficiency tris(8-hydroxyquinoline) aluminum (Alq_3) complexes for organic white-light-emitting diodes and solid-state lighting. *Chem. Eur. J.* **17**, 9076–9082 (2011). https://doi.org/10.1002/chem.201100707

[5] Painuly, D. *et al*. Phase stability and transformation of the α to ε-phase of Alq_3 phosphor after thermal treatment and their photo-physical properties. *J. Phys. Chem. Solids* **121**, 396–408 (2018). https://doi.org/10.1016/j.jpcs.2018.05.035

[6] Hamada, Y. *at al*. Organic electroluminescent devices with 8-hydroxyquinoline derivative-metal complexes as an emitter. *Jpn. J. Appl. Phys.* **32**, 514 (1993). https://doi.org/10.1143/JJAP.32.L514

[7] Ghedini, M., Deda, M. L., Aiello, I. & Grisolia, A. Fine-tuning the luminescent properties of metal-chelating 8-hydroxyquinolines through amido substituents in 5-position. *Inorg. Chim. Acta* **357**, 33–40 (2004). https://doi.org/10.1016/S0020-1693(03)00427-4

[8] Sapochak, L. S. *et al*. Electroluminescent zinc(II) bis(8-hydroxyquinoline): Structural effects on electronic states and device performance. *J. Am. Chem. Soc.* **124**, 6119–6125 (2002). https://doi.org/10.1021/ja0201909

[9] Donze, N., Pechy, P., Gratzel, M., Schaer, M. & Zuppiroli, L. Quinolinate zinc complexes as electron transporting layers in organic light-emitting diodes. *Chem. Phys. Lett.* **315**, 405–410 (1999). https://doi.org/10.1016/S0009-2614(99)01272-5

[10] Du, N., Mei, Q. & Lu, M. Quinolinate aluminum and zinc complexes with multi-methyl methacrylate end groups: Synthesis, photoluminescence, and electroluminescence characterization. *Synth. Metals* **149**, 193–197 (2005). https://doi.org/10.1016/j.synthmet.2005.01.001

[11] Giro, G. *et al*. The role played by cell configuration and layer preparation in LEDs based on hydroxyquinoline metal complexes and a triphenyl-diamine derivative (TPD). *Synth. Met.* **102**, 1018–1019 (1999). https://doi.org/10.1016/S0379-6779(98)01268-5

[12] Hopkins, T. A. Substituted aluminum and zinc quinolates with blue-shifted absorbance/luminescence bands: Synthesis and spectroscopic, photoluminescence, and electroluminescence characterization. *Chem. Mater.* **8**, 344–351 (1996). https://doi.org/10.1021/cm9503442

[13] Sapochak, L. S. *et al.* Effects of systematic methyl substitution of metal (III) tris(*n*-Methyl-8-Quinolinolato) chelates on material properties for optimum electroluminescence device performance. *J. Am. Chem. Soc.* **123**, 6300–6307 (2001). https://doi.org/10.1021/ja010120m

[14] Shukla, V. K. & Kumar, S. Conversion of a green light emitting zinc-quinolate complex thin film to a stable and highly packed blue emitter film. *Synth. Met.* **160**, 450–454 (2010). https://doi.org/10.1016/j.synthmet.2009.11.030

[15] Painuly, D. *et al*. The modification in the photo–physical properties via transformation of synthetic dihydrated Znq_2 to anhydrous $(Znq_2)_4$ tetramer by sublimation process. *Opt. Mater.* **82**, 175–189 (2018). https://doi.org/10.1016/j.optmat.2018.04.044

[16] Jafari, F., Elahi, S. M. & Jafari, M. R. A facile synthesis and opto-electronic characterization of Znq_2 and Alq_3 nano-complexes. *Appl. Phys. A* **124**, 574 (2018). https://doi.org/10.1007/s00339-018-1978-6

[17] Rawat, M., Prakash, S., Singh, C. & Anand, R. S. Synthesis and study of chemical and photo-physical properties of quinolinate aluminum and zinc complexes in organic light emitting diodes (OLEDs). *AIP Conf. Proc.* **1391**, 187–189 (2011). https://doi.org/10.1063/1.3646819

[18] Lim, H. *et al*. Polymeric light-emitting diodes utilizing TPD-dispersed polyimide thin film and organometallic complex. *Proc. SPIE* **3281**, *Polymer Photonic Devices* (1998). https://doi.org/10.1117/12.305439

[19] Sano, T. *et al*. Design of conjugated molecular materials for optoelectronics. *J. Mater. Chem.* **10**, 157–161 (2000). https://doi.org/10.1039/A903239H

[20] Sypniewska, M. *et al*. Tris(8-hydroxyquinoline)aluminium in a polymer matrix as an active layer for green OLED applications. *Opto-Electron. Rev.* **31**, e146105 (2023). https://doi.org/10.24425/opelre.2023.146105

[21] Frisch, M. J. e*t al*. *Gaussian 16, Rev. C.01*. (Gaussian, Inc., Wallingford CT, 2016).

[22] Chai, J.-D. & Head-Gordon, M. Long-range corrected hybrid density functionals with damped atom–atom dispersion corrections. *Phys. Chem. Chem. Phys.* **10**, 6615–6620 (2008). https://doi.org/10.1039/B810189B

[23] Weigend, F. & Ahlrichs, R. Balanced basis sets of split valence, triple zeta valence and quadruple zeta valence quality for H to Rn: Design and assessment of accuracy. *Phys. Chem. Chem. Phys.* **7**, 3297–3305 (2005). https://doi.org/10.1039/B508541A

[24] Bannewart, C., Ehlert, C. & Grimme, S. GFN2-xTB – An acurate and broadly parametrized self-consistent tight-binding quantum chemical method with multipole electrostatics and density-dependent dispersion contributions. *J. Chem. Theory Comput.* **15**, 1652–1671 (2019). https://doi.org/10.1021/acs.jctc.8b01176

[25] Le Bahers, T., Adamo, C. & Ciofini, I. A qualitative index of spatial extent in charge-transfer excitations. *J. Chem. Theory Comput.* **7**, 2498–2506 (2011). https://doi.org/10.1021/ct200308m

[26] Boto, R. A. *et al*. NCIPLOT4: A New Step Towards a Fast Quantification of Noncovalent Interactions. *ChemRxiv.* https://doi.org/10.26434/chemrxiv.9831536.v1 (2019).

[27] Johnson, E. R. *et al*. Revealing noncovalent interactions. *J. Am. Chem. Soc.* **132**, 6498–6506 (2010). https://doi.org/10.1021/ja100936w

[28] Contreras-Garcia, J. *et al*. NCIPLOT: A Program for Plotting Noncovalent Interaction Regions. *J. Chem. Theory Comput.* **7**, 625–632 (2011). https://doi.org/10.1021/ct100641a

[29] Barbosa de Brito, E. B., de Morais, A., Nei de Freitas, J., Valaski, R. & de Fátima Vieira Marques, M. Improved properties of high molar mass poly(9-vinylcarbazole) and performance as a light emitter compared with the commercial PVK. *Mater. Sci. Eng. B* **286**, 116020 (2022). https://doi.org/10.1016/j.mseb.2022.116020

[30] Shahedi, Z., Jafari, M. R. & Zolanvari, A. A., Synthesis of ZnQ_2, CaQ_2, and CdQ_2 for application in OLED: Optical, thermal, and electrical characterizations. *J. Mater. Sci. Mater. Electron.* **28**, 7313–7319 (2017). https://doi.org/10.1007/s10854-017-6417-5

[31] Hien, N. *at al*. Synthesis, structure, photophysical properties and DFT investigation of novel Zn (II) complexes bearing π-extended 8-hydroxyquinoline-derived ligands. *J. Mol. Struct*. **1311**, 138464 (2024). https://doi.org/10.1016/j.molstruc.2024.138464

[32] Knysh, I. *at al*. Reference CC3 excitation energies for organic chromophores: benchmarking TD-DFT, BSE/GW and wave function methods. *J. Chem. Theory Comput*. **20**, 8152–8174 (2024). https://doi.org/10.1021/acs.jctc.4c00906

[33] Jafari, F., Elahi, S. M. & Jafari, M. R. A facile synthesis and optoelectronic characterization of Znq_2 and Alq_3 nano-complexes. *Appl. Phys. A* **124**, 574 (2018). https://doi.org/10.1007/s00339-018-1978-6

[34] Thinh, P. X., Basavaraja, C., Kim, D. G. & Huh, D. S. Characterization and electrochemical behaviors of honeycomb-patterned poly(N-vinylcarbazole)/polystyrene composite films. *Polym. Bull.* **69**, 81–94 (2012). https://doi.org/10.1007/s00289-012-0727-9

[35] Hosseini, S. M., Jashni, E., Jafari, M. R., Van der Bruggen, B. & Shahedi, Z. Nanocomposite polyvinyl chloride-based heterogeneous cation exchange membrane prepared by synthesized ZnQ_2 nanoparticles: Ionic behavior and morphological characterization. *J. Membr. Sci.* **560**, 1–10 (2018). https://doi.org/10.1016/j.memsci.2018.05.007

[36] Bakhshipour, S., Shahedi, Z., Mirahmadi, F., Fereidonnejad, R. & Hesani, M. Effect of different in situ temperatures on the crystallinity and optical properties of green synthesized 8-hydroxyquinoline zinc by saffron extract, *Opt. Contin.* **1**, 1401–1412 (2022). https://doi.org/10.1364/OPTCON.459222

[37] Hu, B.-s., X. *et al*. The effects of crystal structure on optical absorption/photoluminescence of bis (8-hydroxyquinoline) zinc. *Solid State Commun*. **136**, 318–322 (2005). https://doi.org/10.1016/j.ssc.2005.08.021

[38] Kong, F., Liu, J., Li, X. F., An, Y. & Qiu, T. Enhanced emission from Alq_3 in PVK/Alq3 blend films based on resonance energy transfer. *J. Polym. Sci. B: Polym. Phys.* **47**, 1772–1777 (2009). https://doi.org/10.1002/polb.21779

[39] Fan, Y. *et al*. Hydrothermal *in-situ* growth of tris(8-hydroxy-quinolate) aluminum nanorods thin films. *Thin Solid Films* **519**, 7659–7663 (2011). https://doi.org/10.1016/j.tsf.2011.05.015

[40] Popielarski, P., Mosinska, L., Zorenko, T. & Zorenko, Y. Luminescence of tris(8-hydroxyquinoline) aluminium thin films under synchrotron radiation excitation. *J. Lumin.* **261**, 119930 (2023). https://doi.org/10.1016/j.jlumin.2023.119930

[41] Zhao, Y. S. *et al*. Photoluminescence and electroluminescence from tris(8-hydroxyquinoline) aluminum nanowires prepared by adsorbent-assisted physical vapor deposition. *Adv. Funct. Mater.* **16**, 1985–1991 (2006). https://doi.org/10.1002/adfm.200600070

[42] Sypniewska, M. *et al*. Organic LEDs based on bis(8-hydroxyquinoline)zinc derivatives with a styryl group. *Molecules* **28**, 7435 (2023). https://doi.org/10.3390/molecules28217435

[43] Burlov, A. S. *et al*. Synthesis, structure, photo-and electro-luminescent properties of methyl-and alkoxy-substituted 4-methyl-N-[2-(phenyliminomethyl) phenyl] benzenesulfamides and their zinc (II) complexes. *Opt. Mater.* **157**, 116412 (2024). https://doi.org/10.1016/j.optmat.2024.116412

[44] Moraes, E. S. *et al*. Zinc (ii)-heteroligand compounds for wet processing OLEDs: a study on balancing charge carrier transport and energy transfer. *Mater. Adv.* **5**, 7778–7788 (2024). https://doi.org/10.1039/d4ma00581c

Supporting Information

The symmetry of the system leads to the presence of nearly degenerate states. The shorter wavelength part of the absorption spectrum, which is clear for the isolated Znq_2 molecule, with a degenerate signal of relatively weak intensity at 291 nm and two additional almost degenerate strong transitions at 234 and 233 nm, becomes much more complicated when Znq_2 interacts with the PVK polymer chain. The presence of the polymer chain introduces a signal at approximately 259 nm, corresponding to the absorption of the carbazole moiety. Similarly, as in the case of Alq_3:PVK [20], the natural transition orbitals for these signals indicate the charge transfer upon excitation, occurring between the Znq_2 and PVK. Le Bahers indexes for the quantification of the charge transfer characters of the transitions, presented in Table S1, together with the centroids of the charge depletion and charge enhancement upon excitation (Fig. S1), confirm that different parts of the Znq_2:PVK are responsible for the transitions below 300 nm.

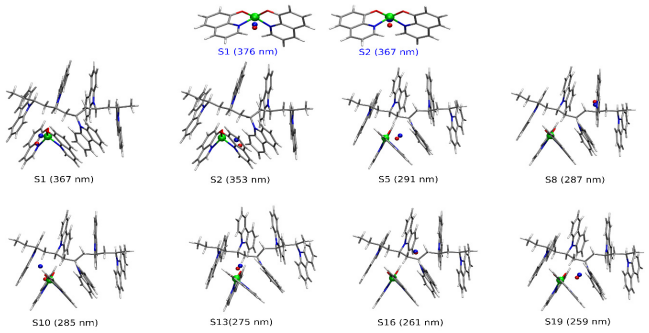

Fig. S1. Charge depletion (blue ball) and charge enhancement (red ball) centroids calculated according to Le Bahers CT indexes for Znq_2 (upper panel) and Znq_2:PVK complex for selected transitions.

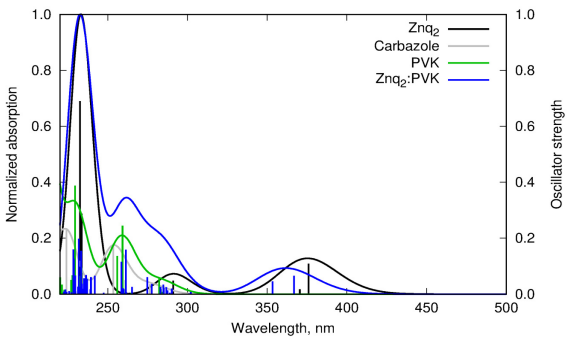

Fig. S2. Vertical absorption spectrum for Znq_2 (black line), carbazole (light grey), PVK model (green), and Znq_2:PVK (blue line) estimated with TD-ωB97X-D/def2-SVP approach.

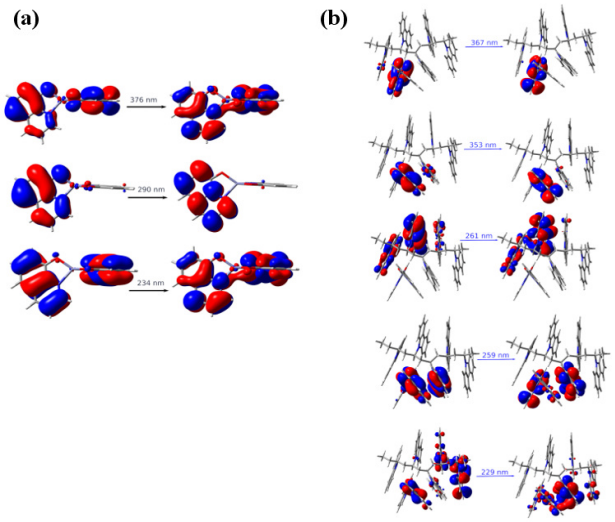

Fig. S3. (a) Natural transition orbitals (NTOs) for the representative most intensive transitions of Znq2, (b) natural transition orbitals for the representative most intensive transitions of Znq2:PVK.

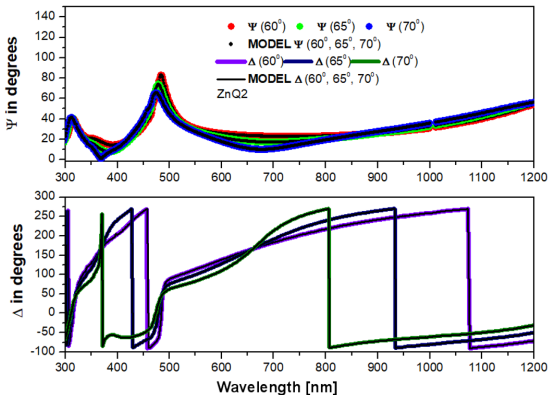

Fig. S4. Spectral dependence of Ψ and Δ azimuths for the unannealed Znq2:PVK layer deposited on the PEDOT:PSS/ITO/glass.

Table S1.
Le Bahers charge transfer parameters, transfer distance *D*, and charge transferred *Q* for the selected most intensive transitions for isolated Znq2 and Znq2:PVK, calculated within the TD-ωB97X-D/def2-SVP approach.

	Znq2					Znq2:PVK			
State	λ [nm]	*f*	*D* [Å]	*Q* [a.u.]	State	λ [nm]	*f*	*D* [Å]	*Q* [a.u.]
S1	376	0.11	0.362	0.656	**S1**	367	0.06	**1.152**	0.828
S2	367	0.02	0.760	0.382	**S2**	353	0.04	0.958	0.806
S3	291	0.04	0.766	0.341	**S5**	291	0.02	**1.412**	0.632
S4	291	0.02	0.440	0.303	**S8**	287	0.02	0.420	0.472
S9	234	0.29	0.736	0.320	**S10**	285	0.03	**1.907**	**1.440**
S10	233	0.69	0.363	0.654	**S13**	275	0.06	1.206	0.488
					S16	261	0.16	0.149	0.355
					S19	259	0.12	**1.282**	0.532
					S34	233	0.15	**1.119**	0.469
					S36	232	0.20	0.368	0.459
					S41	229	0.13	**1.988**	0.809
					S42	228	0.16	**1.675**	0.673